# Effects of Nitrogen Atoms on Mechanical Properties of Graphene by Molecular Dynamics Simulations

Shingo Okamoto and Akihiko Ito

*Abstract*—**We investigated the mechanical properties of nitrogen-containing graphene under tensile loading via molecular dynamics (MD) simulations. In the MD simulation, we used three types of potential functions: the second-generation reactive empirical bond order (REBO) potential for covalent C–C bonds, the Tersoff potential for covalent C–N bonds, and the Lennard–Jones potential for the interlayer interaction of graphite. We studied the effects of nitrogen content and different distributions of nitrogen atoms in graphene on its properties. It was found that nitrogen content of up to 4% had little effect on the mechanical properties of graphene, except when two nitrogen atoms contained in graphene adjoined each other.**

*Index Terms*—**graphene, molecular dynamics, nitrogen, tensile strength**

## I. Introduction

GLOBAL warming and the exhaustion of fossil fuels have recently attracted worldwide attention. This situation necessitates the development of new technologies that take into account environmental problems. Alternative carbon materials are being investigated as potential candidates toward solving these problems owing to their superior mechanical and electrical properties. In particular, graphene and graphite, which are the basic structures in carbon materials, have been found to possess excellent strength (~130 GPa) and the same Young's modulus (~1 TPa) as that of diamond. Therefore, many studies have recently been conducted on graphene and graphite [1], [2]. It is crucial to clarify the mechanical properties of graphene and graphite to develop high-performance carbon materials.

In general, carbon materials derived from raw materials contain impurities such as oxygen, nitrogen, or hydrogen atoms, and these impurities may affect the mechanical and electronic properties of the materials. Recently, Shen and Chen [3], [4] investigated the effects of nitrogen (N) doping on the mechanical properties of ultrananocrystalline diamond (UNCD) films by using molecular dynamics (MD) simulations. They demonstrated that the strength of N-doped UNCD films decreases with increasing density of the dopant N atoms. Similarly, the presence of N atoms may also decrease the strength of graphene and graphite. In our previous work, we investigated the influence of the N atom on the mechanical properties of graphene under tensile loading via MD simulations [5]. In this study, we clarify the influence of three forms of N distribution observed in the graphene structure on mechanical properties of graphene.

Manuscript received May 10, 2012. This work was supported in part by the Ring-Ring project of JKA.

S. Okamoto is with the Graduate School of Science and Engineering, Ehime University, 3 Bunkyo-cho, Matsuyama 790-8577, Japan (e-mail: okamoto.shingo.mh@ehime-u.ac.jp).

A. Ito is with the Graduate School of Science and Engineering, Ehime University, 3 Bunkyo-cho, Matsuyama 790-8577, Japan. He is also with the Composite Materials Research Laboratories, Toray Industries, Inc., Masaki-cho 791-3193, Japan (e-mail: Akihiko_Ito@nts.toray.co.jp).

## II. Method

### A. Potential Function

In this study, we used three types of interatomic potentials: the second-generation reactive empirical bond order (2nd REBO) [6]; Tersoff [7], [8]; and Lennard–Jones potentials. The 2nd REBO potential for covalent C–C bonds is given by (1):

$$E_{REBO} = \sum_i \sum_{j>i} \left[ V_R\left(r_{ij}\right) - B_{ij}^* V_A\left(r_{ij}\right) \right]. \quad (1)$$

The terms $V_R(r_{ij})$ and $V_A(r_{ij})$ denote the pair-additive interactions that reflect interatomic repulsions and attractions, respectively. $B_{ij}^*$ denotes the bond-order term.

The Tersoff potential for covalent C–N bonds is given by (2):

$$V = \frac{1}{2} \sum_{i \neq j} \left[ f_C\left(r_{ij}\right) A_{ij} \exp\left(-\lambda_{ij} r_{ij}\right) - b_{ij} f_C\left(r_{ij}\right) B_{ij} \exp\left(-\mu_{ij} r_{ij}\right) \right], \quad (2)$$

where $b_{ij}$ is the bond-order term that depends on the local environment.

$$b_{ij} = \chi_{ij} \left(1 + \beta^{n_i} \zeta_{ij}^{n_i}\right)^{-1/2n_i}, \quad (3)$$

$$\zeta_{ij} = \sum_{k \neq i,j} f_C\left(r_{ik}\right) g\left(\theta_{ijk}\right), \quad (4)$$

$$g\left(\theta_{ijk}\right) = 1 + \frac{c_i^2}{d_i^2} - \frac{c_i^2}{d_i^2 + \left(h_i - \cos\theta_{ijk}\right)^2}, \quad (5)$$

where $\theta_{ijk}$ is the angle between bonds $ij$ and $ik$.

The parameters $A_{ij}$, $B_{ij}$, $\lambda_{ij}$, and $\mu_{ij}$ depend on the atom type, namely, carbon or nitrogen. For atoms $i$ and $j$ (of different types), these parameters are

$$A_{ij} = \left(A_i \times A_j\right)^{\frac{1}{2}},\ B_{ij} = \left(B_i \times B_j\right)^{\frac{1}{2}} \text{ and} \tag{6}$$

$$\lambda_{ij} = \frac{\left(\lambda_i + \lambda_j\right)}{2},\ \mu_{ij} = \frac{\left(\mu_i + \mu_j\right)}{2}, \tag{7}$$

where the parameters with a single index represent the interaction between atoms of the same type.

The parameter $\chi_{ij}$ in (3) takes into account the strengthening or weakening of the heteropolar bonds. There are no data for the determination of $\chi_{ij}$ for C–N interaction at present. In our model, $\chi_{ij}$ is set to 0.8833 to obtain the lattice constants $a$ and $b$ of the graphitic-$C_3N_4$ orthorhombic structure as 4.10 and 4.70 Å, respectively. From discussions on the N–N interaction, we know that the $N_2$ does not interact with other atoms because of its high binding energy (9.8 eV) and the fact that it diffuses through the crystal and exits the surface. In our model, to keep the $N_2$ stable inside the crystalline structure, $\chi_{N\text{-}N}$ is set to zero [3], [8].

The 2nd REBO and Tersoff potentials contain the same cutoff function $f_c(r)$, as given in (8). It is known that for these potential functions, the interatomic force increases dramatically at $r = R_{\min}$ and approaches zero at $r = R_{\max}$ owing to the discontinuity of the second derivatives of the cutoff function, and this dramatic increase in the interatomic force greatly affects tensile strength. In this work, the cutoff length $R_{\min}$ of both the 2nd REBO and the Tersoff potentials is set to 2.1 Å to avoid a dramatic increase in interatomic forces [9].

$$f_c(r) = \begin{cases} 1, & r < R_{\min} \\ \left\{1 + \cos\left[\dfrac{\pi\left(r - R_{\min}\right)}{R_{\max} - R_{\min}}\right]\right\}/2, & R_{\min} < r < R_{\max} \\ 0, & r > R_{\max} \end{cases}. \tag{8}$$

The interatomic force curves of the C–C and C–N bonds of the $sp^2$ structure are shown in Fig. 1. The force of the C–N bond is stronger than that of the C–C bond. The dramatic increase in the force curve disappears gradually.

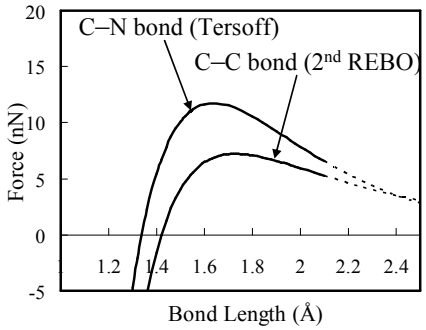


Fig. 1. Interatomic forces of C–C and C–N bonds.

The Lennard–Jones potential for interlayer interaction in the graphitic-$C_3N_4$ model is given by (9):

$$V^{LJ} = 4\varepsilon\left\{\left(\frac{r_0}{r_{ij}}\right)^{12} - \left(\frac{r_0}{r_{ij}}\right)^{6}\right\}. \tag{9}$$

The use of the 2nd REBO and Lennard–Jones potentials are switched according to interatomic distance and bond order [10]. The use of the Tersoff and Lennard–Jones potentials are also switched in the same way.

### *B. Analysis Model*

The crystal structure of orthorhombic graphitic-$C_3N_4$ [11] is shown in Fig. 2. All the covalent bonds are C–N bonds. The unit cell that is enclosed by the box has two lattice constants, $a$ and $b$. The analysis model used in determining $\chi_{ij}$ in the Tersoff potential is shown in Fig. 3. The fundamental cell is composed of six layers of graphitic-$C_3N_4$ sheets, which are stacked in an AB-type sequence. Each layer consists of 48 C atoms and 64 N atoms. Periodic boundary conditions are imposed in all the directions.

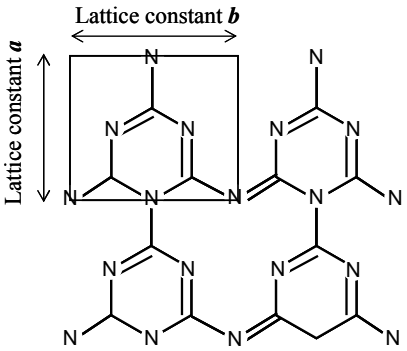


Fig. 2. Orthorhombic structure of graphitic-$C_3N_4$. (The unit cell is enclosed by the box.)

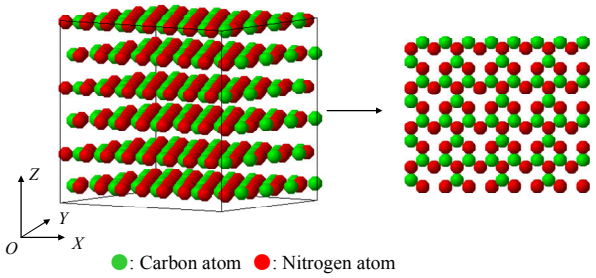


Fig. 3. Configuration of orthorhombic structure of graphitic-$C_3N_4$ used for determining $\chi_{ij}$.

An analysis model of pristine graphene employed under a condition of zigzag orientation consists of 588 C atoms with dimensions identical to those of a real crystallite in typical carbon material, as shown in Fig. 4.

No periodic boundary condition is imposed here so that we may simulate the fracture process. The analysis models consist of two parts. One part is referred to as the active zone, in which the atoms move according to their interactions with neighboring atoms. The other part enclosed by the boxes as shown in Fig. 4 is referred to as the boundary zone in which the atoms are restrained. The thickness $l$ of the boundary zone is $1.5 \times \sqrt{3}a$ for the zigzag tension model, where $a$ is the length of the C=C bond of graphene.

Three types of analysis models were used to investigate the effect of the distributional form of N atoms on mechanical properties of graphene. The first set of models contains uniform distribution models. The analysis models for uniformly distributed N atoms in graphene are shown in Fig. 5. The C atoms in the active zone of the graphene model, as

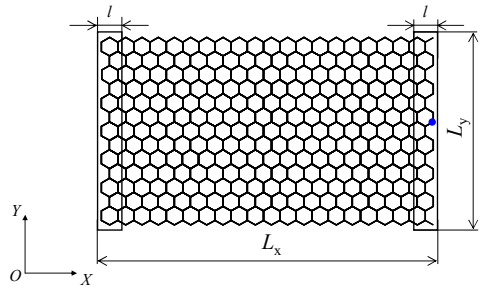


● The atom fixed in the Y direction during an initial relaxation.

Fig. 4. Configuration of graphene under zigzag tension.

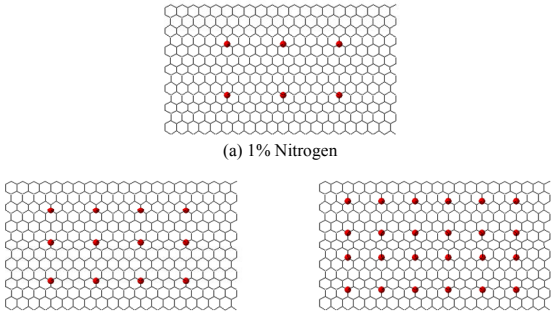

(a) 1% Nitrogen

(b) 2% Nitrogen (c) 4% Nitrogen

Fig. 5. Analysis models for N-containing graphene for different N content.

shown in Fig. 4, are replaced with the N atoms such that the distance between neighboring N atoms is uniform.

Three cases of differing N content, namely, 1%, 2%, and 4%, were investigated. The second set of models includes random distribution models in which N atoms do not adjoin each other. In these analysis models, random C atoms in the active zone are replaced with N atoms of a pseudorandom number so that N atoms do not adjoin each other.

The third set of models includes random distribution models containing randomly distributed N atoms and including two adjoining ones. In these analysis models, random C atoms in the active zone are replaced with N atoms so that only the two N atoms adjoin each other.

### C. MD Simulation

All the MD calculations employed the velocity Verlet method to calculate the time integral of the equations of motion of atoms. The velocities of all atoms were adjusted simultaneously using the velocity scaling method [12] in order to control the temperature of the object by the preset temperature $T_{SET}$. The mass of C atoms, $m_C$, and that of N atoms, $m_N$, are $1.9927 \times 10^{-26}$ kg and $23.253 \times 10^{-27}$ kg, respectively. The time step is 1.0 fs.

*Determination of the $\chi_{C-N}$ in Tersoff Potential*

We determined the parameter $\chi_{C-N}$ in the Tersoff potential by calculating the lattice constants of graphitic-$C_3N_4$ via MD simulations under constant pressure and temperature, that is, an isothermal–isobaric (NPT) ensemble at $1.0 \times 10^{-17}$ K.

The pressure $P_{IJ}$ and stress $\sigma_{IJ}$ for the directions $X$, $Y$, and $Z$, given by (10) and (11) are determined by calculating the kinetic energies of and interatomic forces on atoms in the fundamental cell:

$$P_{IJ} = \frac{1}{v}\left( \sum_{i \in v} m\overline{V_I^i V_J^i} + \sum_{i \in v} \overline{I^i F_J^i} \right) \quad (I=X, Y, Z; J=X, Y, Z), \tag{10}$$

$$\sigma_{IJ} = \frac{1}{v}\left( \sum_{i \in v} m\overline{V_I^i V_J^i} + \sum_{i \in v} \overline{I^i F_J^i} \right) - P \quad (I=X, Y, Z; J=X, Y, Z), \tag{11}$$

where v denotes the volume, $m$ is either $m_C$ or $m_N$, and $P$ denotes the external pressure. The pressure is adjusted by controlling the volume of the fundamental cell using (12) such that all the components of the output stress tensor for graphitic-$C_3N_4$ are zero:

$$L_I\left(1 + \alpha_I\left(P_{II} - P_{SET}\right)\right) \to L_I, \quad (I=X, Y, Z), \tag{12}$$

where $L_I$ denotes the length of the fundamental cell in the $I$ direction. $P_{SET}$ is the preset external pressure and $\alpha_I$ is an appropriate constant. In this study, $P_{SET}$ is set to 1 atm and $\alpha_I$ is set to 0.03.

The initial positions of the atoms are given such that the analysis model becomes identical to the crystal structure of graphitic-$C_3N_4$. All the atoms are relaxed in unloaded states for 19,000 MD simulation steps. Then, the lattice constants $a$ and $b$ are sampled for 2,000 MD simulation steps and averaged.

*Tension of N-Containing Graphene*

Next, we investigated the mechanical properties of N-containing graphene by using MD simulations under a constant volume and temperature, that is, the canonical (NVT) ensemble at 300 K.

The atomic stress acting on each atom is calculated to obtain the stress–strain curves and to visualize stress distribution during tensile loadings. The atomic stress $\sigma^i{}_J$ for each of the $X$, $Y$, and $Z$ directions of $J$ is obtained by calculating the kinetic energies of atom $i$, the interatomic force acting on it, and the volume occupied by it, as given in (13):

$$\sigma^i{}_J = \frac{1}{\Omega^i}\left( m\overline{V^i{}_J V^i{}_J} + \overline{J^i F^i{}_J} \right). \tag{13}$$

Here, $\Omega^i$ denotes the volume occupied by atom $i$, which is referred to as atomic volume. This volume is calculated by averaging the volume of all atoms in the initial structure of each system. $m$ can be either $m_C$ or $m_N$. $F^i{}_J$ denotes the interatomic force acting on atom $i$ from the neighboring atoms. The global stress of an analysis model is calculated by averaging over all atoms in each system.

The initial positions of the atoms are given such that the analysis model becomes identical to the crystal structure of N-containing graphene at 300 K. First, the atoms of the analysis model are relaxed until the stresses are stabilized for 10,000–14,000 MD simulation steps. The atoms in the active zone are relaxed in all three directions. The atom shown by a blue circle in Fig. 4 is relaxed in the $X$ direction only. The atoms in the left-hand side boundary zone are relaxed in the $Y$ direction only. The atoms in the right-hand side boundary zone, except the atom shown by a blue circle, are relaxed in only the $X$ and $Y$ directions. After the atoms are relaxed, constant displacements are applied to the atoms in the boundary zones to simulate uniaxial tensile loading in the $X$

direction. The atoms in the boundary zones are restrained in the *X* and *Z* directions. The atoms in the active zone of the analysis model are relaxed for all the directions, and those in the boundary zones are relaxed only in the *Y* direction for 7,000 MD simulation steps. The strain increment $\Delta\varepsilon$ is 0.004. The Young's moduli are obtained from the slopes of the straight lines in the range, where the relation between the stress and strain is linear, and tensile strengths are given by the peak of the nominal-stress–nominal-strain curves.

## III. Results and Discussion

### A. Determination of the $\chi_{C-N}$ in Tersoff Potential

The lattice constants *a* and *b* with the parameter $\chi_{C-N}$ are shown in Fig. 6. The relations between both the lattice constants *a* and *b* and $\chi_{C-N}$ are found to be linear for $\chi_{C-N}$ from 0.8 to 1.0. $\chi_{C-N}$ was determined to be 0.8833 when *a* and b were 4.10 and 4.70 Å, respectively, on the basis of the work of Alves *et al*. [11].

### B. Mechanical Properties of N-Containing Graphene

Examples of the stress–strain curves of graphene containing uniformly distributed N atoms are shown in Fig. 7. The calculated tensile strengths and Young's moduli are listed in Table I.

The increase in stress is delayed for the N-containing graphene. This delay is attributed to the N atoms that prevent flatness of the graphene sheet. It is found that the tensile strength and Young's modulus of the graphene sheet do not change much with a change in N content.

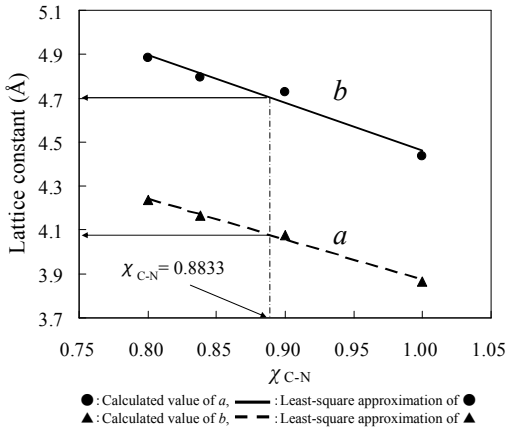


Fig. 6. Lattice constants *a* and *b* as a function of parameter $\chi_{C-N}$.

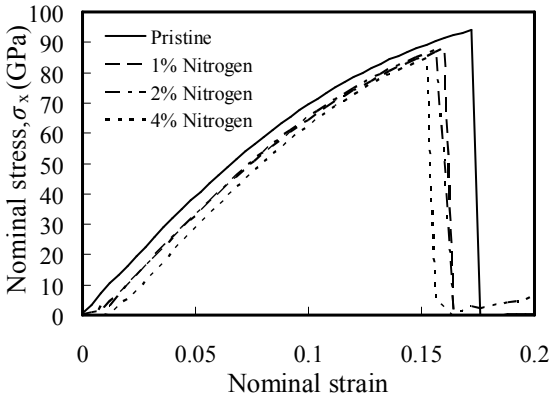


Fig. 7. Stress-strain curves of graphene containing uniformly distributed N atoms.

Snapshots taken during tensile loadings are shown in Fig. 8. In each case, fractures occur because of cleavage of the C–C bond, which is in proximity to a C–N bond.

Examples of the stress–strain curves of graphene containing randomly distributed N atoms that do not adjoin each other are shown in Fig. 9. The calculated tensile strengths and Young's moduli are listed in Table II. Decrease in tensile strengths and fracture strain is almost the same as that in graphene containing a similar amount of uniformly distributed N atoms. The Young's modulus changes little with a change in N content.

Snapshots taken during tensile loadings are shown in Fig. 10. In all cases, fractures occur because of cleavage of the C–C bond, which is in proximity to a C–N bond. The same is observed in graphene containing uniformly distributed N atoms.

Examples of the stress–strain curves of graphene containing randomly distributed N atoms and including two adjoining ones are shown in Fig. 11. The calculated tensile strengths and Young's moduli are listed in Table III. The decline in tensile strength is larger than in the case of the random distribution in which N atoms do not adjoin each other.

TABLE I
Mechanical Properties of Graphene Containing Uniformly Distributed N Atoms

| Nitrogen content (%) | Tensile strength (GPa) | Young's modulus (GPa) |
|---|---|---|
| 0 | 94 | 786 |
| 1 | 88(−6.3%) | 758(−3.5%) |
| 2 | 87(−7.4%) | 774(−1.5%) |
| 4 | 84(−10%) | 772(−1.7%) |

Values in parentheses represent the differences between the pristine and N-containing materials.

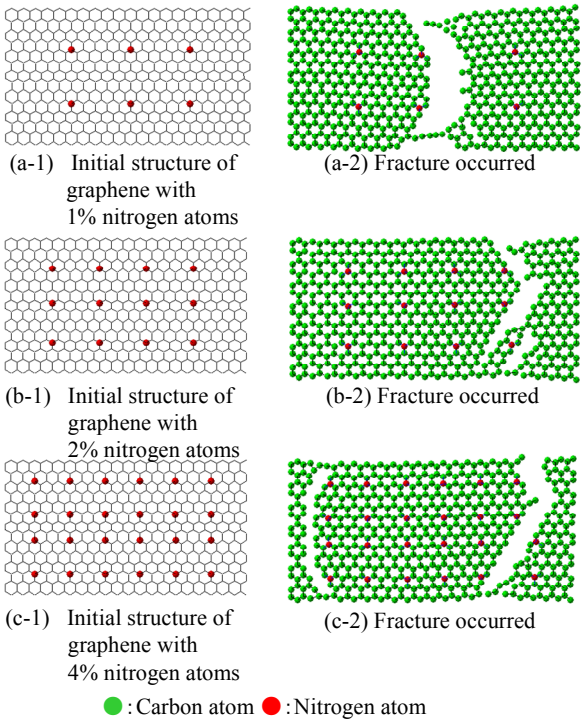


Fig. 8. Structures before tensile loading and after fracture for grapheme containing uniformly distributed N atoms.

On the other hand, the Young's modulus is almost the same as that for graphene containing randomly distributed N atoms and including two adjoining ones.

The relation between tensile strength and N content is shown in Fig. 13. For the random distribution, the average values of the two results calculated using models with different N arrangements are plotted. The error bar (the elongated I) represents the range between two values. There is no difference in the tensile strength between the uniform distribution and random distribution having no adjoined N atoms. For the random distribution with two adjoining N

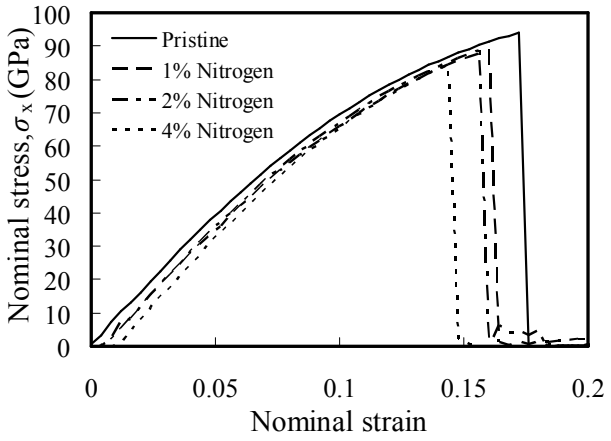


Fig. 9. Stress–strain curves of graphene containing randomly distributed N atoms that do not adjoin each other.

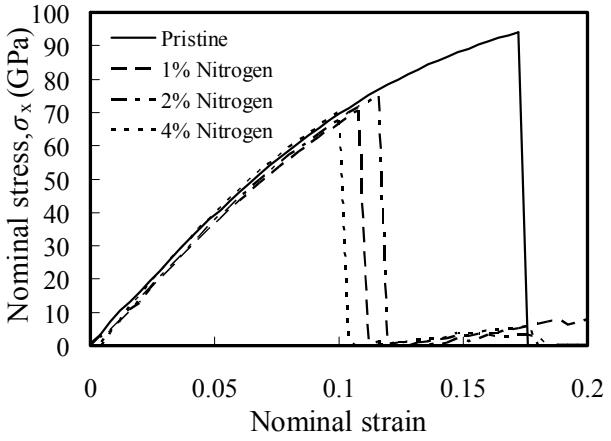


Fig. 11. Stress–strain curves of graphene containing randomly distributed N atoms and including two adjoining ones.

TABLE II
MECHANICAL PROPERTIES OF GRAPHENE CONTAINING RANDOMLY DISTRIBUTED N ATOMS THAT DO NOT ADJOIN EACH OTHER

| Nitrogen content (%) | Tensile strength (GPa) | Young's modulus (GPa) |
|---|---|---|
| 0 | 94 | 786 |
| 1 | 89(−5.3%) | 773(−1.6%) |
| 2 | 87(−7.4%) | 801(+1.9%) |
| 4 | 82(−12%) | 822(+4.5%) |

Values in parentheses represent the differences between the pristine and N-containing materials.

TABLE III
MECHANICAL PROPERTIES OF GRAPHENE CONTAINING RANDOMLY DISTRIBUTED N ATOMS AND INCLUDING TWO ADJOINING ONES

| Nitrogen content (%) | Tensile strength (GPa) | Young's modulus (GPa) |
|---|---|---|
| 0 | 94 | 786 |
| 1 | 64(−31%) | 770(−2.0%) |
| 2 | 69(−26%) | 776(−1.2%) |
| 4 | 69(−26%) | 823(+4.7%) |

Values in parentheses represent the differences between the pristine and N-containing materials.

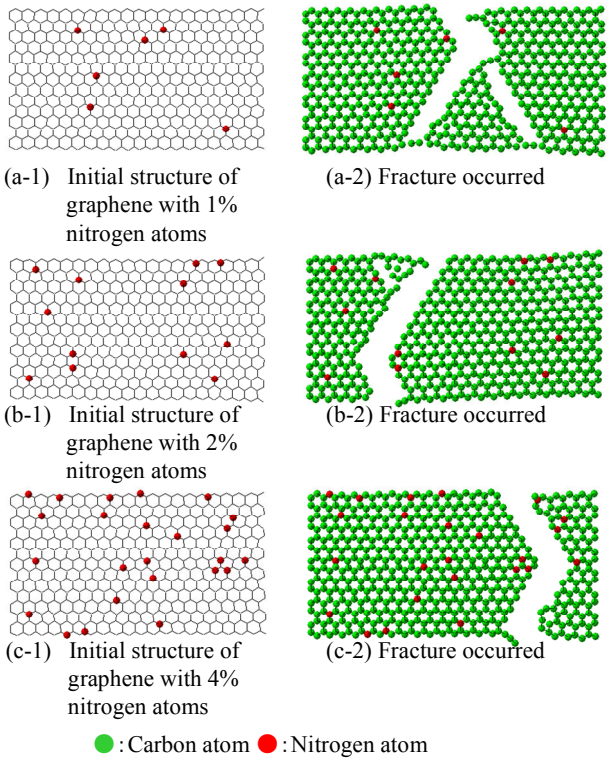


Fig. 10. Structures before tensile loading and after fracture for graphene containing randomly distributed N atoms that do not adjoin each other.

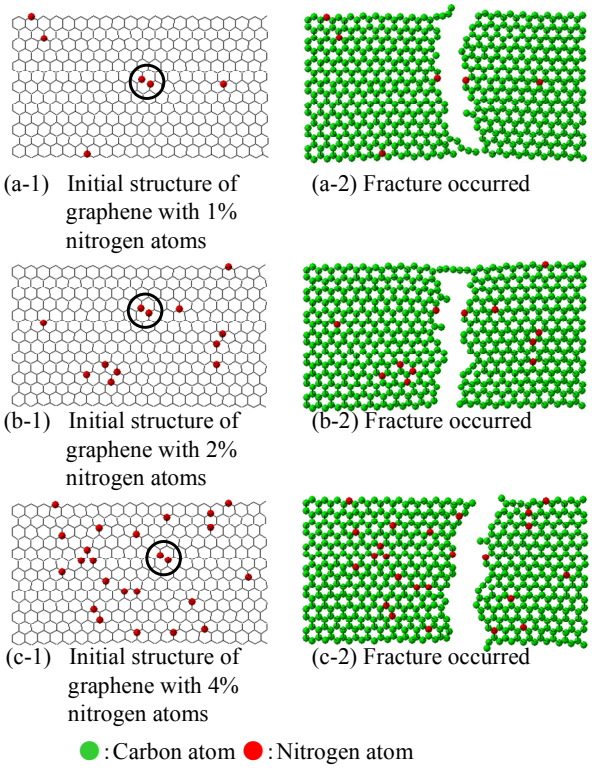


Fig. 12. Structures before tensile loading and after fracture for graphene containing randomly distributed N atoms and including two adjoining ones. The two adjoining N atoms are circled.

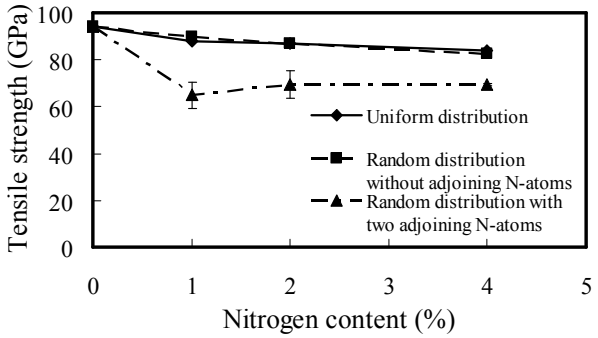


Fig. 13. Tensile strengths as a function of content of uniformly or randomly distributed N atoms.

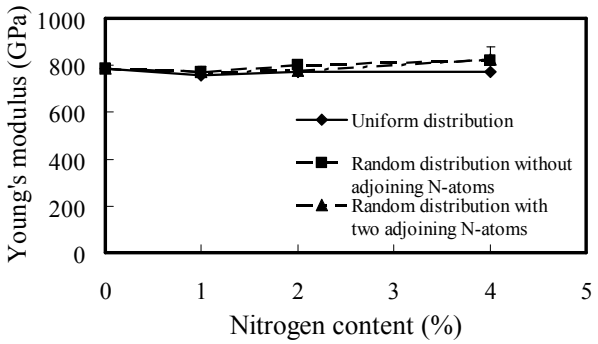


Fig. 14. Young's moduli as a function of content of uniformly or randomly distributed N atoms.

atoms, the decline in the tensile strength is larger than it is in the other two cases and the decline is independent of N content. From these results, it was found that the presence of two adjoining N atoms in graphene affect the tensile strength considerably. The relation between the Young's modulus and the N content is shown in Fig. 14. For all the three cases, Young's modulus barely changes with changing N content.

### *C. Influence of Distance between Two N Atoms on Tensile Strength of Graphene*

Examples of stress–strain curves of graphene containing two N atoms located at an interval *d* are shown in Fig. 15. The calculated tensile strengths and Young's moduli are listed in Table IV.

We found that the tensile strength decreases with decreasing distance between two N atoms. The decrease in tensile strength in the case of pristine graphene is about 25% when two N atoms adjoin each other, i.e., when *d* is 1.76 Å.

The relation of the tensile strengths with the distance between two N atoms is shown in Fig. 16. The larger the distance of separation between two N atoms, the higher is the tensile strength. This relation is almost constant when *d* exceeds 2.38 Å. When *d* between two N atoms is 1.76 Å, the strength almost agrees with that for graphene containing randomly distributed N atoms and including two adjoining ones.

When two N atoms are located alternately in the form N–C–N (i.e., when *d* is 2.38 Å), the strength almost agrees with that of graphene containing uniformly distributed N atoms or that of randomly distributed N atoms that do not adjoin each other at a N content of 4%.

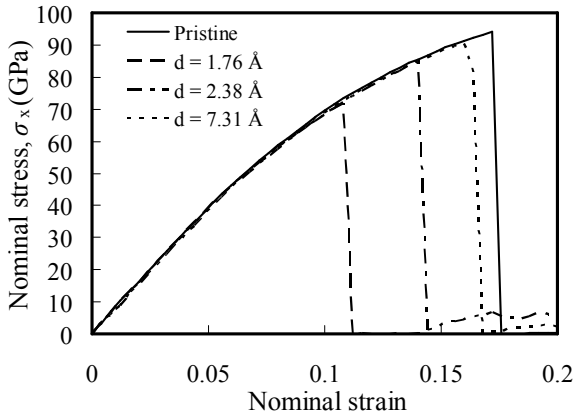


Fig. 15. Stress–strain curves of graphene containing two N atoms located at an interval *d*.

TABLE IV
MECHANICAL PROPERTIES OF GRAPHENE CONTAINING TWO N ATOMS

| *d* (Å) | Tensile strength (GPa) |
|---|---|
| 1.76 | 71 |
| 2.38 | 84 |
| 7.31 | 90 |

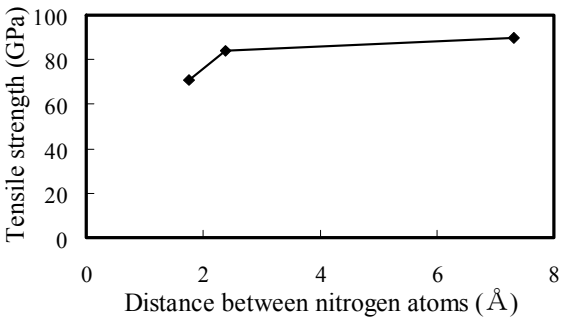


Fig. 16. Relation of tensile strength and the distance between two N atoms.

Snapshots taken during the tensile loadings are shown in Fig. 17. In the case of *d* = 1.76 Å ((a-1)–(a-4)), fracture occurs at the point where two N atoms adjoin each other, similar to the case of graphene containing randomly distributed N atoms and including two adjoining ones (Fig. 12). Stress does not concentrate on N atoms before fracture (a-2). Instead, stress concentrates on the two C atoms located alternately after each N atom. In the case of *d* = 2.38 and 7.31 Å ((b-1)–(b-4) and (c-1)–(c-4), respectively), the stress concentrates on the N atom and its neighboring C atoms. Fracture starts at the cleavage of the C–C bond adjoining the N atom and not at a C–N bond, because of the stronger binding force of the C–N bond.

## IV. CONCLUSION

We performed MD simulations for tensile loadings of graphene containing N atoms in order to investigate the effect of the N atom on the mechanical properties of graphene. As a result, we found that neither the strength nor Young's modulus changes much for a N content of up to 4% unless two N atoms present in graphene adjoin each other. We demonstrated that the presence of two N atoms in graphene affects tensile strength considerably.

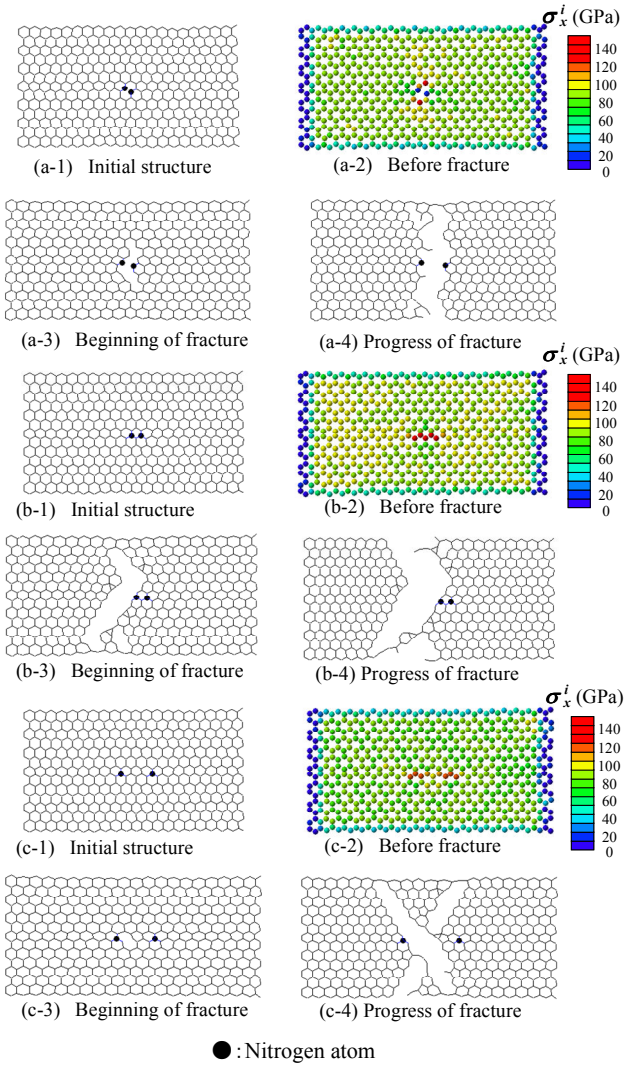


Fig. 17. Stages of fracture progress in graphene containing two N atoms at different intervals *d*: 1.76 Å ((a-1)–(a-4)); 2.38 Å ((b-1)–(b-4)); and 7.31 Å ((c-1)–(c-4)).

## REFERENCES


[1] R. Granatab, V. B. Shenoy, and R. S. Ruoff, "Anomalous strength characteristics of tilt grain boundaries in graphene," *Science*, vol. 330, pp. 946–948, Nov. 2010.

[2] J. R. Xiao, J. Staniszewski, and J. W. Gillespie, Jr., "Tensile behaviors of graphene sheets and carbon nanotubes with multiple Stone–Wales defects," *Mater. Sci. Eng. A*, vol. 527, pp. 715–723, Jan. 2010.

[3] L. Shen and Z. Chen, "An investigation of grain size and nitrogen-doping effects on the mechanical properties of ultrananocrystalline diamond films," *Int. J. Sol. Struct.*, vol. 44, pp. 3379–3392, May 2007.

[4] L. Shen and Z. Chen, "A study of mechanical properties of pure and nitrogen-doped ultrananocrystalline diamond films under various loading conditions," *Int. J. Sol. Struct.*, vol. 46, pp. 811–823, Feb. 2009.

[5] S. Okamoto and A. Ito, "Investigation of mechanical properties of nitrogen-containing graphene using molecular dynamics simulations," *Lecture Notes in Engineering and Computer Science: Proceedings of the International MultiConference of Engineers and Computer Scientists 2012*, *IMECS 2012*, 14–16 March, 2012, Hong Kong, pp. 350–355.

[6] D. W. Brenner, O. A. Shenderova, J. A. Harrison, S. J. Stuart, B. Ni, and S. B. Sinnott, "A second-generation reactive empirical bond order (REBO) potential energy expression for hydrocarbons," *J. Phys.: Condens. Matter*, vol. 14, pp. 783–802, Jan. 2002.

[7] J. Tersoff, "Modeling solid-state chemistry: Interatomic potentials for multicomponent systems," *Phys. Rev. B*, vol. 39, no. 8, pp.5566–5568, Mar. 1989.

[8] J. Tersoff, "Structural properties of amorphous silicon nitride," *Phys. Rev. B*, vol. 58, no. 13, pp. 8323–8328, Oct. 1998.

[9] O. A. Shenderova, D. W. Brenner, A. Omeltchenko, X. Su, L. H. Yang, and M. Young, "Atomistic modeling of the fracture of polycrystalline diamond," *Phys. Rev. B*, vol. 61, no. 6, pp. 3877–3888, Feb. 2000.

[10] S. J. Stuart, A. B. Tutein, and J. A. Harrison, "A reactive potential for hydrocarbons with intermolecular interactions," *J. Chem. Phys.*, vol. 112, no. 14, pp. 6472–6486, Jan. 2000.

[11] I. Alves, G. Demazeau, B. Tanguy, and F. Weill, "On a new model of the graphitic form of $C_3N_4$," *Solid State Commun.*, vol. 109, pp. 697–701, Mar. 1999.

[12] L. V. Woodcock, "Isothermal molecular dynamics calculations for liquid salts," *Chem. Phys. Lett.*, vol. 10, pp. 257–261, Aug. 1971.